JUSTC

Article

http://justc.ustc.edu.cn

Received: October 09, 2022; Accepted: November 29, 2022

Investigating the mechanisms driving the seasonal variations in surface $PM_{2.5}$ concentrations over East Africa with the WRF-Chem model

Nkurunziza Fabien Idrissa[1,2], Chun Zhao[1,3,4] ✉, Qiuyan Du[3], Shengfu Lin[3], Kagabo Safari Abdou[5], Weichen Liu[3], and Xiaodong Wang[3]

[1]*School of Earth and Space Sciences, University of Science and Technology of China, Hefei 230026, China;*
[2]*School of Public Health, Environmental Health Science Dept., University of Rwanda (UR-CMHS), Kigali, Rwanda;*
[3]*Deep Space Exploration Laboratory, University of Science and Technology of China, Hefei 230026, China;*
[4]*CAS Center for Excellence in Comparative Planetology, University of Science and Technology of China, Hefei 230026, China;*
[5]*School of Science, Physics Dept., University of Rwanda (UR-CST), Kigali, Rwanda*

✉Correspondence: Chun Zhao, Chun Zhao, E-mail: chunzhao@ustc.edu.cn

Graphical abstract

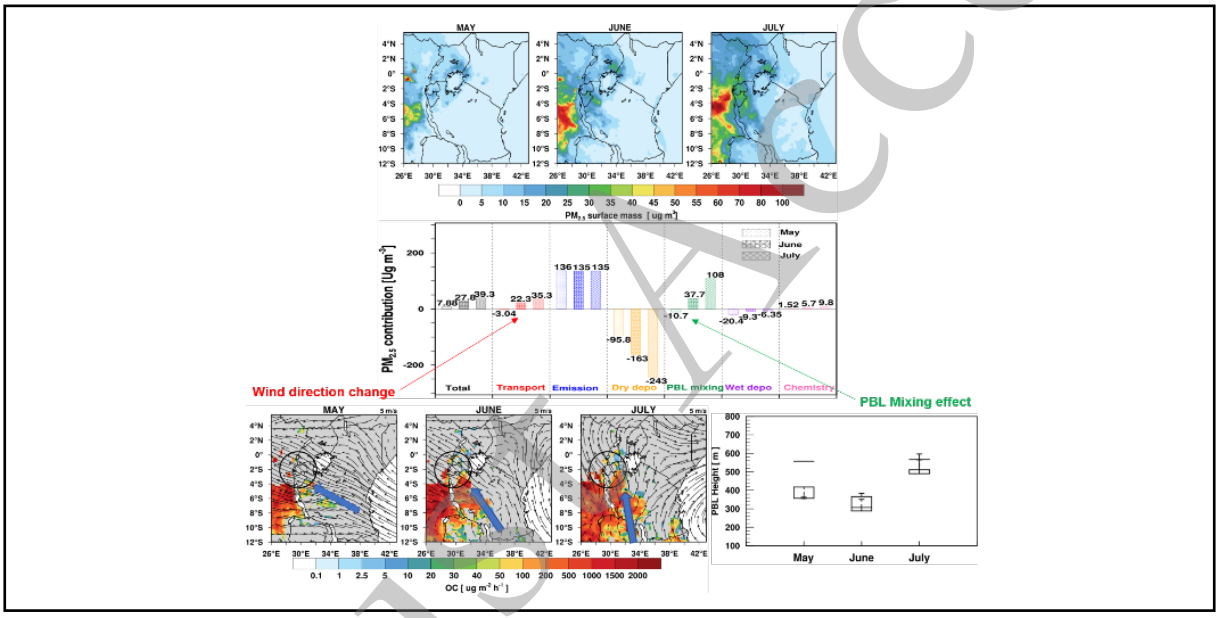

Spatial distribution surface $PM_{2.5}$ concentrations and the mechanism driving its seasonal variations.

Public summary

- WRF-Chem simulations and in situ observations of surface PM2.5 concentrations were combined to study the seasonal variation over East Africa.
- Analysis of contributions from multiple physical and chemical processes found transport, PBL mixing and wet and dry deposition to be driving mechanisms in the variation in surface concentration.
- Wind direction changes transported aerosols to the region, and turbulent mixing with decreased rainfall increased the surface concentration from May to July.

Citation: Idrissa N F, Zhao C, Du Q Y, et al. Investigating the mechanisms driving the seasonal variations in surface $PM_{2.5}$ concentrations over East Africa with the WRF-Chem model. *JUSTC*, **2023**, 53(5): . DOI: 10.52396/JUSTC-2022-0142

JUSTC

Article

http://justc.ustc.edu.cn

Received: October 09, 2022; Accepted: November 29, 2022

Investigating the mechanisms driving the seasonal variations in surface $PM_{2.5}$ concentrations over East Africa with the WRF-Chem model

Nkurunziza Fabien Idrissa[1,2], Chun Zhao[1,3,4] ✉, Qiuyan Du[3], Shengfu Lin[3], Kagabo Safari Abdou[5], Weichen Liu[3], and Xiaodong Wang[3]

[1]*School of Earth and Space Sciences, University of Science and Technology of China, Hefei 230026, China;*
[2]*School of Public Health, Environmental Health Science Dept., University of Rwanda (UR-CMHS), Kigali, Rwanda;*
[3]*Deep Space Exploration Laboratory, University of Science and Technology of China, Hefei 230026, China;*
[4]*CAS Center for Excellence in Comparative Planetology, University of Science and Technology of China, Hefei 230026, China;*
[5]*School of Science, Physics Dept., University of Rwanda (UR-CST), Kigali, Rwanda*

✉Correspondence: Chun Zhao, Chun Zhao, E-mail: chunzhao@ustc.edu.cn

Cite This: *JUSTC*, **2023**, 53(5): (14pp) Read Online SI Supporting Information

Abstract: Most previous studies on surface $PM_{2.5}$ concentrations over East Africa focused on short-term in situ observations. In this study, the WRF-Chem model combined with in situ observations is used to investigate the seasonal variation in surface $PM_{2.5}$ concentrations over East Africa. WRF-Chem simulations are conducted from April to September 2017. Generally, the simulated AOD is consistent with satellite retrieval throughout the period, and the simulations depicted the seasonal variation in $PM_{2.5}$ concentrations from April to September but underestimated the concentrations throughout the period due to the uncertainties in local and regional emissions over the region. The composition analysis of surface $PM_{2.5}$ concentrations revealed that the dominant components were OIN and OC, accounting for 80% and 15% of the total concentrations, respectively, and drove the seasonal variation. The analysis of contributions from multiple physical and chemical processes indicated that the seasonal variation in surface $PM_{2.5}$ concentrations was controlled by the variation in transport processes, PBL mixing, and dry and wet deposition. The variation in $PM_{2.5}$ concentrations from May to July is due to wind direction changes that control the transported biomass burning aerosols from southern Africa, enhanced turbulent mixing of transported aerosols at the upper level to the surface and decreased wet deposition from decreased rainfall from May to July.

Keywords: East Africa; WRF-Chem; Real-time Affordable Multi-Pollutant sensor (RAMPs); Seasonal Variation; Surface $PM_{2.5}$ concentrations

CLC number: **Document code:** A

1 Introduction

Aerosols are an important component of the Earth-ocean-atmosphere system. Natural and anthropogenic aerosols are well known for their significant impacts on human health, climate change, atmospheric visibility, stratospheric ozone depletion, acid deposition, and photochemical smog [1, 2]. Aerosols have been reported to have a detrimental effect on human health through the deterioration of air quality in the planetary boundary layer, as they are the major causes of haze, smog, fog, and dust storms [3–5]. Air pollution in cities is more severe in low- and middle-income countries (LMICs) than in developed countries and leads to over 92% of global pollution-related deaths. The WHO reported in 2013 that one in eight premature deaths globally was currently linked to poor air quality [6]. Despite the burden caused by air pollution in LMICs, it is still poorly studied [7]. East Africa has a population of 126 million, which accounts for 10% of the continental population of East African countries [8]. The rapid growth of the population in this region is associated with industrialization, urbanization, continued use of biomass as a domestic source of energy, growing ownership of motor vehicles, inadequate and deteriorated transport infrastructure, and unpaved roads [9]. All these factors have contributed to air pollution in the region. The near-surface concentrations of fine particulate matter (PM) in the cities of East Africa were reported to be relatively higher than those in the cities of Europe and North America, which were approximately 100 μg m^{-3} and 20 μg m^{-3}, respectively [7, 10]. For instance, [11] reported that the 24-h mean PM concentration in the city of Kampala was 132.1 μg m^{-3}.

The air quality of East Africa is determined not only by the source characteristics but also by the climate of the region. There is a bimodal rainfall pattern corresponding to the two wet seasons, March to May (MAM), namely, ‘long rains’, and October to December (OND), as “short rains”, over East Africa. This region recognizes the arid period of scarce rain

DOI: 10.52396/JUSTC-2022-0142
JUSTC, **2023**, 53(5):

from June to September (JJAS) as the "dry season" [12, 13]. This regional climate of East Africa is strongly associated with sea surface temperature variability [14−16]. It is also largely influenced by the equatorial mass flow "trade winds" and their zone of interference as the Inter-Tropical Convergence Zone (ITCZ) [17]. In addition, subtropical highs, especially the Mascarene High, modulate the seasonal rainfall variability over the region [18]. Furthermore, some studies have also linked the rainfall variability of the region with the El Niño Southern Oscillation (ENSO) [19]. The characteristics of near-surface $PM_{2.5}$ concentrations over East Africa have been neglected compared to other regions of the continent.

Most studies on PM in East Africa have mainly focused on the source apportionment and temporal variability of PM based on short-term in situ observations [7, 10, 11, 20, 21]. Many of those studies demonstrated temporal variations in PM in different cities of East Africa and showed that the surface $PM_{2.5}$ concentrations were higher in the dry season and lower in the wet season. [10] studied the concentrations of $PM_{2.5}$ and PM_{10} and their compositions of polycyclic aromatic hydrocarbons (PAHs) and nitrated PAHs (NPAHs) from April to June. Their results showed a higher surface concentration of $PM_{2.5}$ and PM_{10} in the urban and roadside samples than in the rural samples during the dry season, while the surface PAH concentrations were higher at the rural sites during the wet season in Rwanda, East Africa. [7] carried out a study on $PM_{2.5}$ and PM_{10} at urban roadside, urban background, and rural sites during February-March and found that the concentrations were higher at roadside and urban sites than at rural sites. Previous studies [11, 21] measured PM2.5, nitrogen dioxide (NO_2), sulfur dioxide (SO2), and ozone (O3) concentrations in two Ugandan cities and reported higher concentrations at industrial sites and near unpaved roads than at residential sites and near paved roads and commercial areas during July. [21] measured $PM_{2.5}$ and $PM_{10,}$ including their carbonaceous composition, during the dry season of 2005 and wet season of 2006 in Dar es Salaam and found that the PM concentration was higher in the dry local season than in the wet local season.

Although previous studies have contributed to some understanding of the seasonal variability in near-surface PM over East Africa with observations [7, 10, 11, 21], there have been very few studies investigating the mechanisms driving the temporal variation in near-surface $PM_{2.5}$ concentrations over East Africa, particularly for the seasonal variation in near-surface $PM_{2.5}$. Numerical modeling is widely used to understand various mechanisms of observed phenomena. Previous studies have used atmospheric models to investigate aerosols and their impacts over North and West Africa, mainly for dust [22–24], and over Central and Southern Africa, mainly for anthropogenic and biomass burning aerosols [15, 25, 26]. Most modeling studies over East Africa have focused only on the variability of meteorological fields such as rainfall, moisture, and temperature [27–31]. To date, very few studies have focused on the modeling performance of surface $PM_{2.5}$ and have investigated the mechanisms driving the seasonal variation in near-surface PM concentrations over East Africa.

This calls for a comprehensive modeling study of the mechanisms of the seasonal transition of near-surface PM concentrations over East Africa. Therefore, this study aims to contribute to the understanding of the seasonal variation in near-surface $PM_{2.5}$ in the East Africa region through numerical modeling. The study applies the widely used regional model Weather Research Forecast coupled with Chemistry (WRF-Chem) to examine the observed seasonal variation in surface $PM_{2.5}$ concentrations in Kigali city from April to September 2017 over East Africa. The simulations are evaluated with available observations and used to investigate the mechanisms driving the seasonal variability in surface PM2.5 concentrations. The specific objectives of the study are (1) to examine the spatial and temporal variations in surface $PM_{2.5}$ concentrations over East Africa and (2) to investigate the impacts of meteorological fields on the seasonal variation in near-surface $PM_{2.5}$ concentrations. The rest of the paper is organized as follows: in the next section, we describe the WRF-Chem model, numerical experiments, anthropogenic emissions, and observations. The results are analyzed and presented in Section 3. The conclusions can be found in Section 4.

2 Methodology

2.1 Model description and experimental setup

WRF-Chem, a nonhydrostatic atmospheric model that simulates trace gases and aerosols with meteorological fields [32−34], is used. In this study, the version of WRF-Chem updated by the University of Science and Technology of China (USTC version of WRF-Chem) is used. This USTC version of WRF-Chem includes some additional capabilities, such as the diagnosis of the radiative forcing of aerosol species, land surface coupled VOC biogenic VOC emissions, aerosol-snow interaction, and the diagnosis of contributions of the individual process such as transport, emission, dry and wet deposition, PBL mixing to the concentration of PM compared with the publicly released version [35−39] Aerosol components were simulated by the Model for Simulating Aerosol Interactions and Chemistry (MOSAIC) together with CBM-Z (carbon bond mechanism); the MOSAIC scheme includes physical and chemical processes of nucleation, condensation, coagulation, aqueous phase chemistry and water uptake by aerosols. The aerosol components include ammonium (NH_{4+}), black carbon (BC), nitrate (NO_{3-}), mineral dust, organic matter (OM), sea salt, sulfate (SO_4^{2-}), and other inorganics (OIN). This study uses a sectional approach where aerosols are distributed into 8 discrete size bins with MOSAIC [40]. The dry deposition of aerosol mass and number were both simulated following the approach of [41], which includes both particle diffusion and gravitational effects. Wet removal of aerosols by grid-resolved stratiform clouds/precipitation includes in-cloud removal and below-cloud removal by impaction and interception [42]. Convective transport and wet removal of aerosols by cumulus follow [43]. The experiments use the Morrison 2-moment cloud microphysical scheme [44], Yonsei University (YSU) planetary boundary layer parameterization [45], Kain-Fritsch convective scheme [46], and Community Land Model version 4 (CLM4) for the land surface scheme. Aerosol radiative feedback is coupled with the Rapid Radiative Transfer Model (RRTMG) [47, 48] for both SW and LW radiation as im-

DOI: 10.52396/JUSTC-2022-0142
JUSTC, **2023**, 53(5):

plemented by [23]; optical properties and direct radiative forcing of individual aerosol species in the atmosphere are diagnosed following the methodology described in [49b].

The WRF-Chem simulations are performed with two nested domains (one-way nesting), an outer domain covering all of Africa using 265×235 grid cells (20°W~50°E and 38°S~38°N) and an inner domain of 157×154 grid cells (26°E~43°E and 12°S~6°N) with horizontal resolutions of 36 km and 12 km, respectively (Figure 1). The inner domain roughly covers the region of East Africa. WRF-Chem is configured with 40 vertical σ-levels with the model top pressure at 10 hPa. The simulation period starts from March 25 to September 30, 2017. The results from April 1st to September 30th are analyzed. The period of April-May is considered the wet season, and the period of June-September is the dry season. Meteorological initial and lateral boundary conditions are derived from the NCEP Final reanalysis data with 1×1 degree horizontal resolution and 6-hour temporal resolution. Modeled u and v component wind and sea surface temperature are nudged toward the reanalysis data with a nudging timescale of 6 h [50–52].

2.2 Emissions

Anthropogenic emissions for both domains are obtained from the Hemisphere Transport of Air Pollution version-2 (HTAPv2) at a 0.1×0.1 horizontal resolution with a monthly temporal resolution for 2010 (Fig. 2a) [53]. Biomass burning emissions were obtained from the Fire Inventory from NCAR (FINN) with hourly temporal resolution and 1 km horizontal resolution (Fig. 2c) [54] and were vertically distributed following the injection heights suggested by [55] for the Aerosol Inter-Comparison project (AeroCom). Based on the magnitude retrieved AOD and considering the uncertainties of the FINN emission inventory, biomass burning emissions are increased by a factor of 4 in this study. Sea salt emission follows [43a], which includes the correction of particles with a radius less than 0.2 mm [56] and the dependence of sea salt emission on sea surface temperature [57]. The dust emission flux is calculated with the GOCART dust emission formula [58] as implemented by Zhao et al. (2010) (Fig. 2b). The emitted dust particles are partitioned into eight aerosol size bins following the theoretical expression based on the physics of scale-invariant fragmentation of brittle materials derived by [59]. More details about the dust emission scheme coupled with the mosaic aerosol scheme in WRF-Chem can be found in [23, 24, 43].

2.3 Datasets

2.3.1 *Satellite retrievals*

MODIS

The Moderate Resolution Imaging Spectrometer (MODIS) instrument was launched on the Earth Observation System and Terra and Aqua platforms in 1999 and 2002, respectively. MODIS instruments are considered the key instruments for atmospheric, land and ocean remote science [60], which are designed as passive imaging radiometers and measure reflected solar and emitted thermal radiation in 36 bands across a 2330 km swath and provide nearly daily global coverage at the equator and overlap between higher latitudes with high spatial resolution ranging from 250 m at the 0.66 μm band, 500 m at the 0.47 μm and 2.1 μm bands, and 1 km at the 11 μm bands [61].

MODIS onboard the Terra platform crosses the equator at ~10:45 am local time, while MODIS onboard the Aqua platform crosses the equator at ~1:30 pm local time [61]. MODIS Collection 6.1 is an updated version of Collection 6, especially for aerosol retrievals over urban areas and with uncertainty estimates. It includes three products based on different

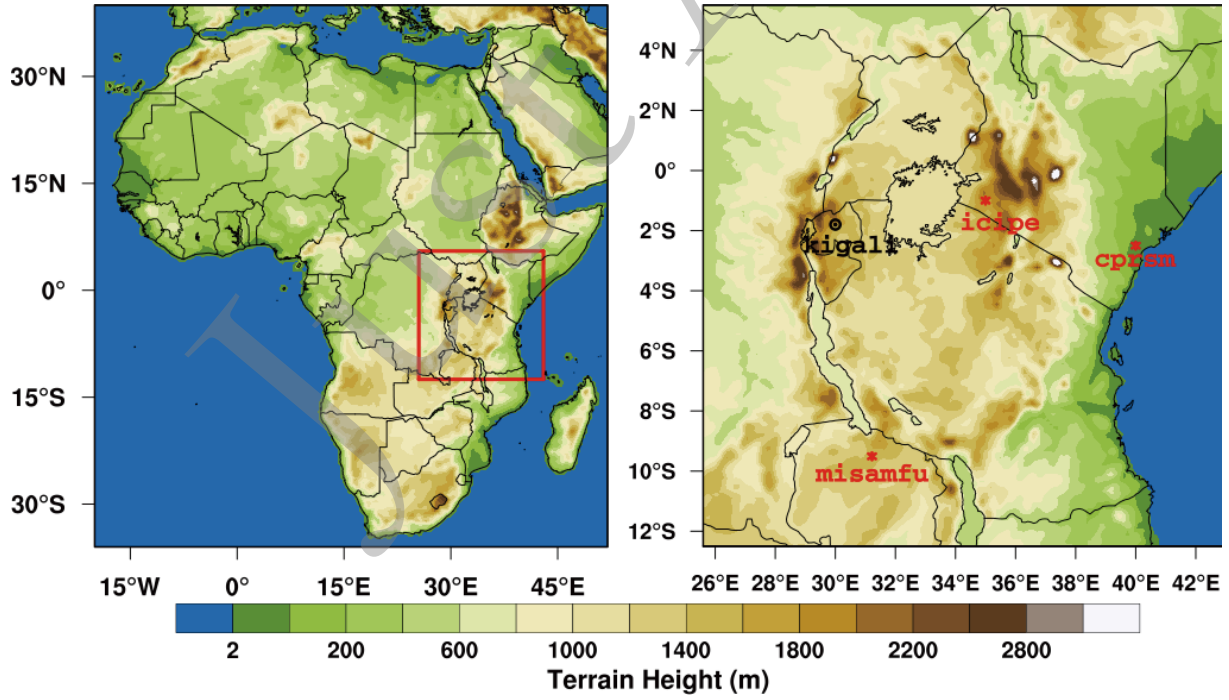

Fig. 1. Domain overview and elevation (left, d01), East Africa (right, d02) with locations of AERONET sites (red stars) and Kigali city (black point).

DOI: 10.52396/JUSTC-2022-0142
JUSTC, **2023**, 53(5):

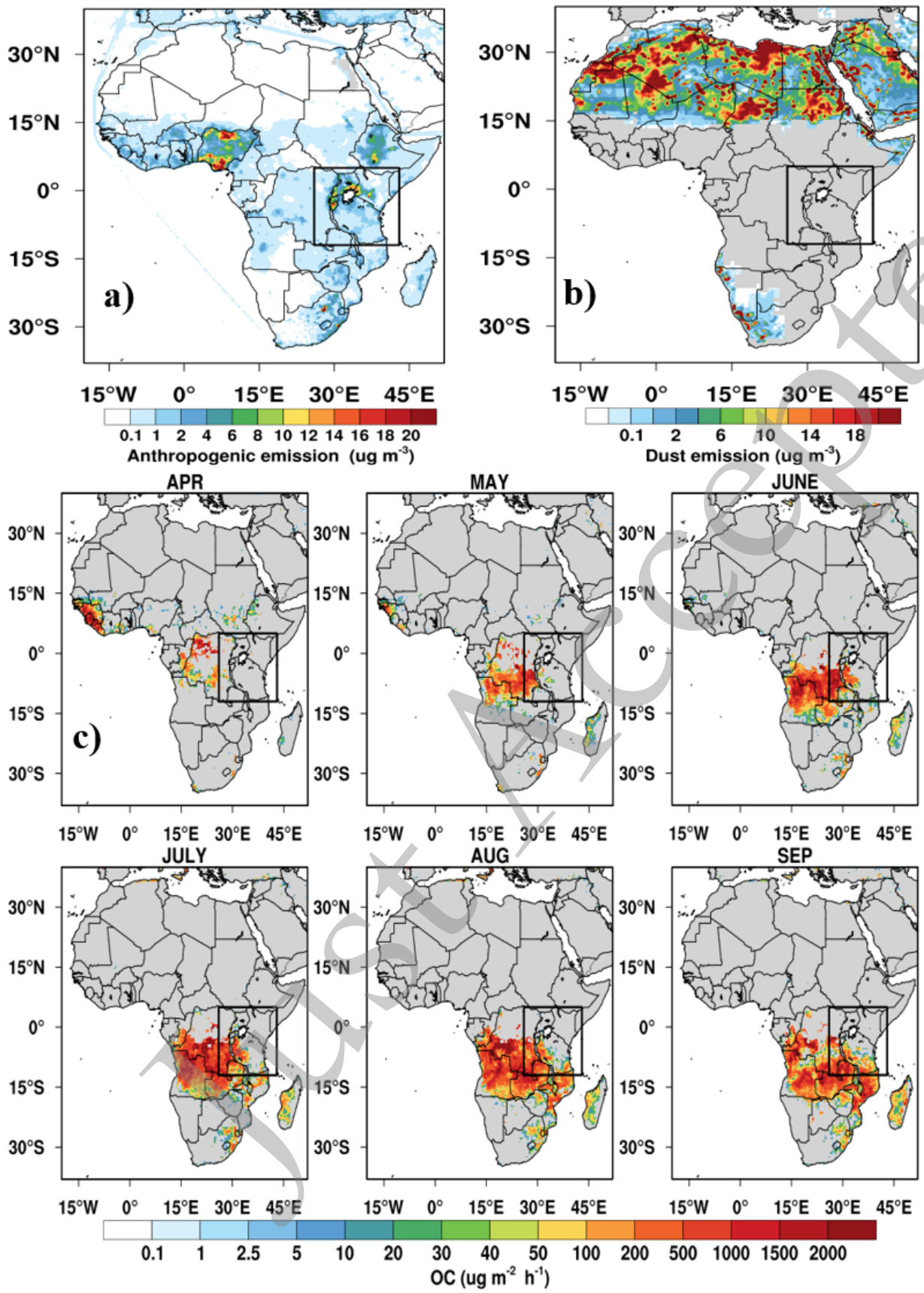

Fig. 2. (a) Anthropogenic emissions for the African continent (d01) and East Africa (d02). (b) Dust emissions over Africa (domain d01). (c) Biomass burning emissions (OC) for domain d01 (Africa) and domain d02 (East Africa); the black box represents domain d02.

DOI: 10.52396/JUSTC-2022-0142
JUSTC, **2023**, 53(5):

algorithms, namely, Deep Blue (DB), Dark Target (DT), and Deep Blue Combined (referring to the merged DT-DB product). DB covers land, and DT covers both land–water bodies at nadir spatial resolutions of 3 km and 10 km. The MODIS level-2 atmospheric aerosol product provides the retrieved ambient aerosol optical properties, quality assurance, and other parameters globally over the ocean and land. In this study, the MODIS Terra level-2 Deep Blue Collection 6.1 retrievals of aerosol optical depth (AOD) at 550 nm of 10×10 km horizontal resolution are downloaded from the NASA Earth data portal and used for analysis [62]. When comparing the modeled AOD with MODIS retrievals, the model results are sampled at the satellite overpass time and location.

MISR

The multiangle imaging spectroradiometer (MISR) instrument was launched aboard the NASA Terra platform in 2000. MISR was designed to retrieve tropospheric aerosol properties at nine distinct zenith angles in four spectral bands centered at 446 nm, 558 nm, 672 nm, and 866 nm. At each of the nine view angles spread out in the 70° forward direction and 70° afterwards. The MISR's unique blend technique of directional and spectral data enables it to retrieve tropospheric AOD over bright surfaces of high reflection, such as desert areas [63]. MISR performs aerosol retrieval over land utilizing the presence of spatial contrasts to separate surface-leaving and atmospheric path radiances. The surface leaving radiation field is then used to determine the best fitting aerosol compositional models and associated AOD by comparing the results with synthesized values that are calculated from predefined aerosol compositional models, each consisting of a mixture of prescribed basic aerosol components. MISR onboard the Terra platform passes over the equator at ~10:45 am local time. MISR Level 2 aerosol optical depth (AOD) retrievals at 558 nm are used in this study. When compared with the MISR products, the simulated AODs are sampled in the same overpass time as Terra.

2.3.2 *Ground measurements*

AERONET

The Aerosol Robotic Network provides more than 100 globally distributed Cimel sun photometers (automated radiometers) established and maintained by NASA [64], which record aerosol optical properties around the globe. Radiometers take the measurements of direct sun and diffuse radiances at 15-30 minute intervals of the spectral ranges of 340-1640 nm and 440-1020 nm, respectively. In this study, we use the AOD at 675 nm at 3 sites in the region of East Africa (CPRSM Malindi, 40°E, 2.99°S; ICIPE, 34.20°E, 0.43°S; MISAMFU, 86.56°E, 28.21°N) for comparison with the modeling results. The available AOD retrievals used are level 1.5 for the same period of the simulation results (see the supporting information, Fig. S1).

RAMP

Real-time affordable multipollutant sensors (RAMPs) were developed in partnership with Carnegie Mellon University's Center for Atmospheric Particle Studies (CAPS) and SenSevere [65]. RAMPs measured $PM_{2.5}$, carbon monoxide (CO), nitrogen dioxide (NO2), sulfur dioxide (SO2), ozone (O3), relative humidity (RH), and temperature (T). More details about the RAMPs can be found in [66]. In collaboration with Carnegie Mellon University and the University of Rwanda, three sites were installed in 3 different locations within the city of Kigali.

The first site was installed in the College of Science Technology (CST), which is located at an elevation of 1554 m (1.9585°S, 30.0643°E) uphill on a plateau in the city on the top of the building. The main sources of particle pollutants reaching this site are related to traffic roads, coal and fuel burning, and primary commercial and residential sources. The second site of the Gacuriro estate (1.9222°S, 30.1010°E) at an elevation of 1466 m is approximately 4 km northeast of the CST site, which is mainly surrounded by residential areas. The third site of the Belle-Vue estate (1.9268°S, 30.0918°E) is at an elevation of 1450 m within 6 km southeast of the Gacuriro estate site, which is also surrounded by residential areas. Both sites were characterized by residential sources. The measurements were recorded from April 2017 to April 2018, and this study uses observations of $PM_{2.5}$ from April 2017 to September 2017 to evaluate WRF-Chem simulations.

3 Results

3.1 Seasonal variation in column-integrated PM

Figure 3 presents the spatial distributions of the monthly average of column-integrated $PM_{2.5}$ from the simulations of domain 2. There is an evident increase in $PM_{2.5}$ mass loading from April (in the rainy season) to September (end of the dry season). The period of April and May was characterized by low concentrations over most areas during the rainy season (referred to as AM in this study), whereas the period of June, July, August and September was characterized by high concentrations mostly spread over the western and southwestern regions during the dry season. The western and southwestern parts of the domain have higher concentrations, which is related mainly to the high emissions from biomass burning in the area (Fig. 2). Generally, the $PM_{2.5}$ mass loading increases from 10 $\mu g \cdot m^{-2}$ in April to the highest value of 60 $\mu g \cdot m^{-2}$ in July and declines afterwards to 30 $\mu g \cdot m^{-2}$ in September over the city of Kigali.

The spatial patterns of AOD at 550 nm from the satellite retrievals and the WRF-Chem simulations over East Africa from April to September 2017 are presented in Figure 4. The spatial distribution of monthly mean AOD represents patterns of high and low AOD, showing distinct features of aerosol loading in different regions of East Africa. Both MODIS and MISR AOD show consistent spatial patterns of AOD. The monthly variation in AOD is related to the monthly (seasonal) climatic conditions and anthropogenic activities. High aerosol loadings (AOD greater than 0.35) were observed during June, July, August, and September (JJAS, local dry season), whereas relatively lower aerosol loadings (AOD less than 0.2) were observed in April and May (MAM, local wet season). High (low) AOD values (April, May) characterize the period as a moderately polluted environment (clean environment) [67]. The high AOD observed during the JJAS period over the western and southwestern regions is attributed to in-

DOI: 10.52396/JUSTC-2022-0142
JUSTC, **2023**, 53(5):

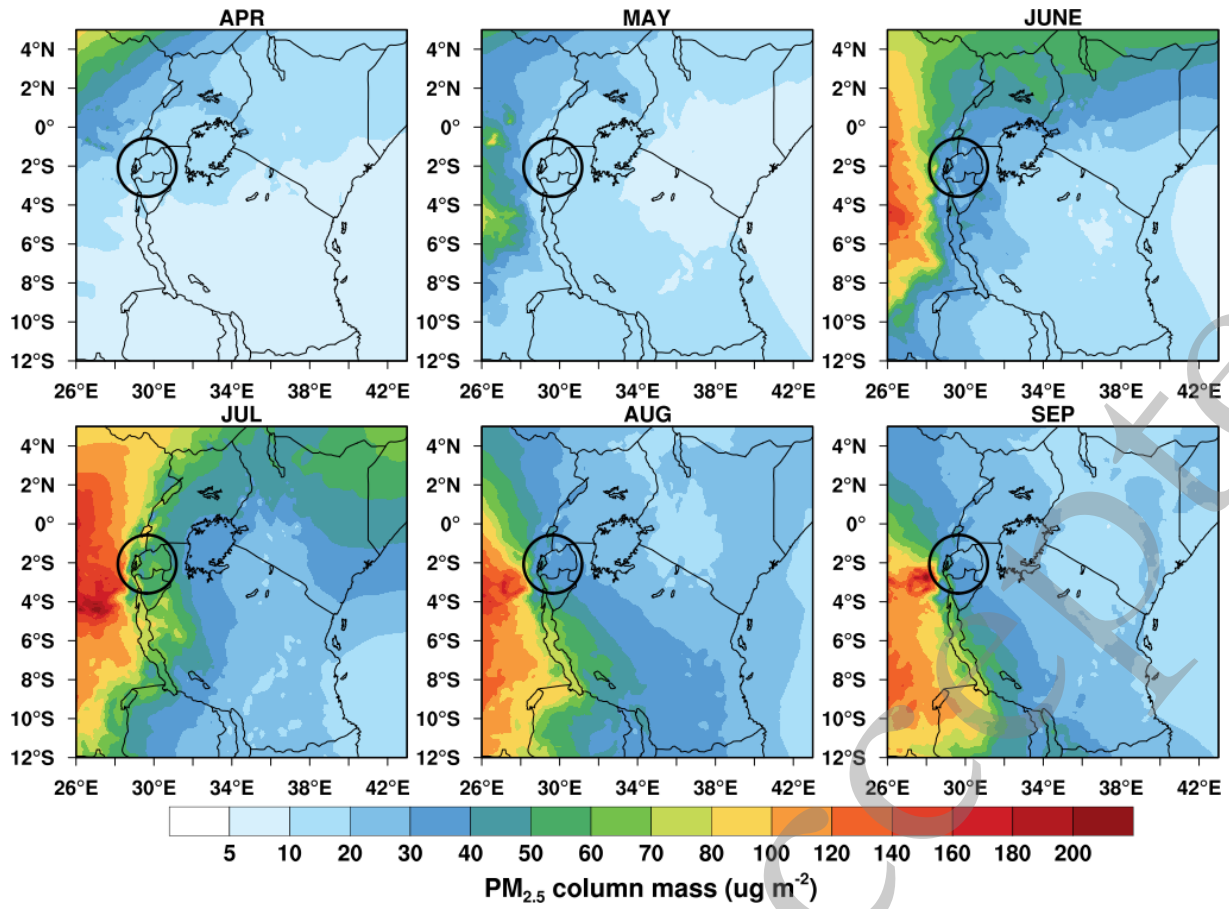

Fig. 3. Spatial distribution of the integrated column of $PM_{2.5}$ mass concentrations averaged for each month over East Africa from the simulation of domain 2 for the April-September period. The black circle shows the region over Rwanda.

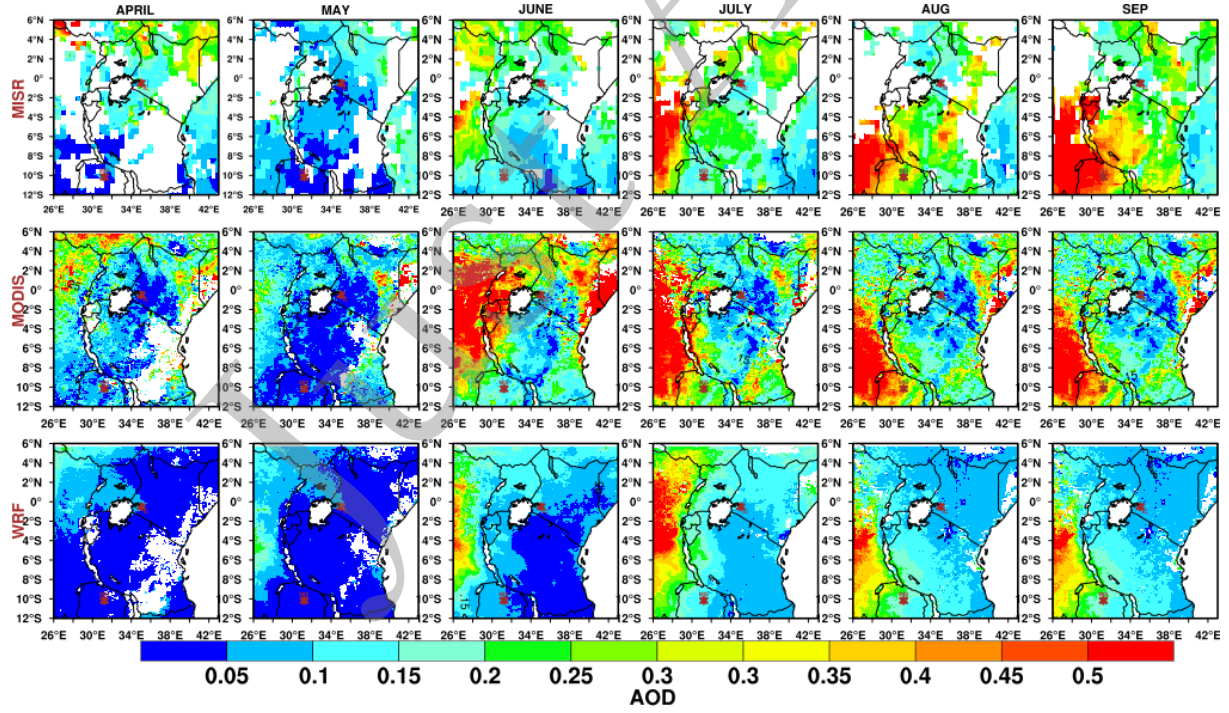

Fig. 4. Spatial distribution of averaged AOD at 550 nm from retrievals of MISR, MODIS Terra, and simulated AOD from WRF-chem over East Africa. Brown dots show the AERONET sites (IC: icipe 34.02°E, 0.43°S; MS: Msamfu, 31.22°E, 10.17°S) for the April-September period. The model results are sampled at the time and locations of the MODIS retrievals. The blank area in the plots means that no data are available.

DOI: 10.52396/JUSTC-2022-0142
JUSTC, **2023**, 53(5):

creased anthropogenic activities, such as cultivation and biomass burning, enhancing the emission of smoke [68]. The semi-arid areas of the northeast region showed high AOD retrieved from the satellites and were associated with locally emitted dust aerosols that were also transported from the Sahara and Arabian Peninsula [69, 70]. The low AOD observed during the AM period over most areas is linked with rainout (suppressing emission of aerosols from the ground) and washout (removal of aerosols from the atmosphere by rains) [71]. Although the WRF-Chem simulation captured the seasonal variations in AOD from satellites (MODIS, MISR), the simulated AOD is apparently lower than the retrieved AOD in August and September even after scaling biomass burning by 4 and dust emissions by 1.25. This underestimation may be attributed to the underestimation of dust and biomass burning emissions near East Africa in these two months. It is also noteworthy that the MODIS-retrieved AOD is higher than that of MISR.

3.2 Seasonal variations in surface $PM_{2.5}$ concentration

Figure 5 shows the spatial distributions of the monthly mean surface $PM_{2.5}$ concentration from the simulations. The monthly means of observed $PM_{2.5}$ averaged over the city of Kigali from three stations are collocated with the simulated surface $PM_{2.5}$ concentration. The eastern and coastal regions exhibit lower surface $PM_{2.5}$ concentrations than other parts of the domain, consistent with the spatial pattern of the total column mass loading. During the rainy season (here referred to as April-May), surface $PM_{2.5}$ exhibits concentrations ranging between 5 $\mu g \cdot m^{-3}$ and 25 $\mu g \cdot m^{-3}$. During the dry season (referred to as June-September, JJAS), the spatial variation is larger, with a higher concentration over the southwestern region above 70 $\mu g \cdot m^{-3}$ and an average ranging between 25 $\mu g \cdot m^{-3}$ and 60 $\mu g \cdot m^{-3}$. The WRF-Chem simulations underestimated the surface $PM_{2.5}$ concentrations throughout the period (AM- JJAS), as can be observed from comparison with collocated station ground $PM_{2.5}$ concentration loading.

Figure 6 shows the daily variations in the surface $PM_{2.5}$ concentration of the observations and WRF-Chem for 6 months (April-September). The average observed $PM_{2.5}$ concentration shows a temporal variation ranging from 20 $\mu g \cdot m^{-3}$ to 40 $\mu g \cdot m^{-3}$ during April-June and 40 $\mu g \cdot m^{-3}$ to 95 $\mu g \cdot m^{-3}$ during July September (Fig. 6a). Overall, the observed $PM_{2.5}$ exhibits a low (peak) concentration of 10 $\mu g \cdot m^{-3}$ (80 $\mu g \cdot m^{-3}$) in May (July). The low concentration in May is associated with heavy rainfall during the wet season [72]. The WRF-Chem simulations show a temporal variation ranging from 10 $\mu g \cdot m^{-3}$ to 30 $\mu g \cdot m^{-3}$ during April-June and 20 $\mu g \cdot m^{-3}$ to 40 $\mu g \cdot m^{-3}$ during July September. The simulations underestimate the $PM_{2.5}$ concentration in the entire period of April-September. However, the simulations can capture the seasonal variation well, such as the dramatic increase in concentration during May-June-July. In particular, the simulations are also able to reproduce the pollution episodes throughout the period, show-

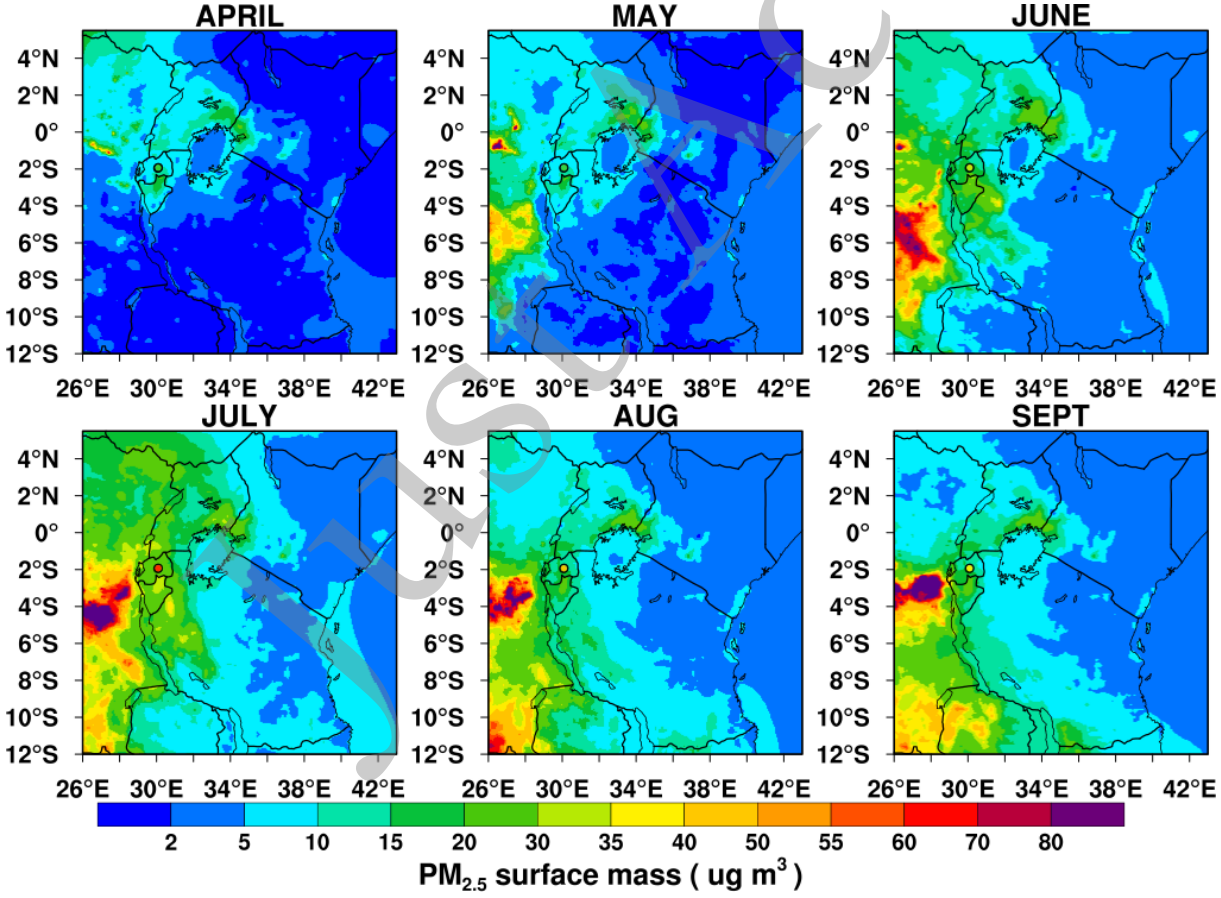

Fig. 5. Spatial distribution of surface $PM_{2.5}$ concentrations from the WRF-Chem simulations collocated with average $PM_{2.5}$ concentrations from observations over Kigali city for the April-September period. Filled circles represent the observed $PM_{2.5}$ concentrations.

DOI: 10.52396/JUSTC-2022-0142
JUSTC, **2023**, 53(5):

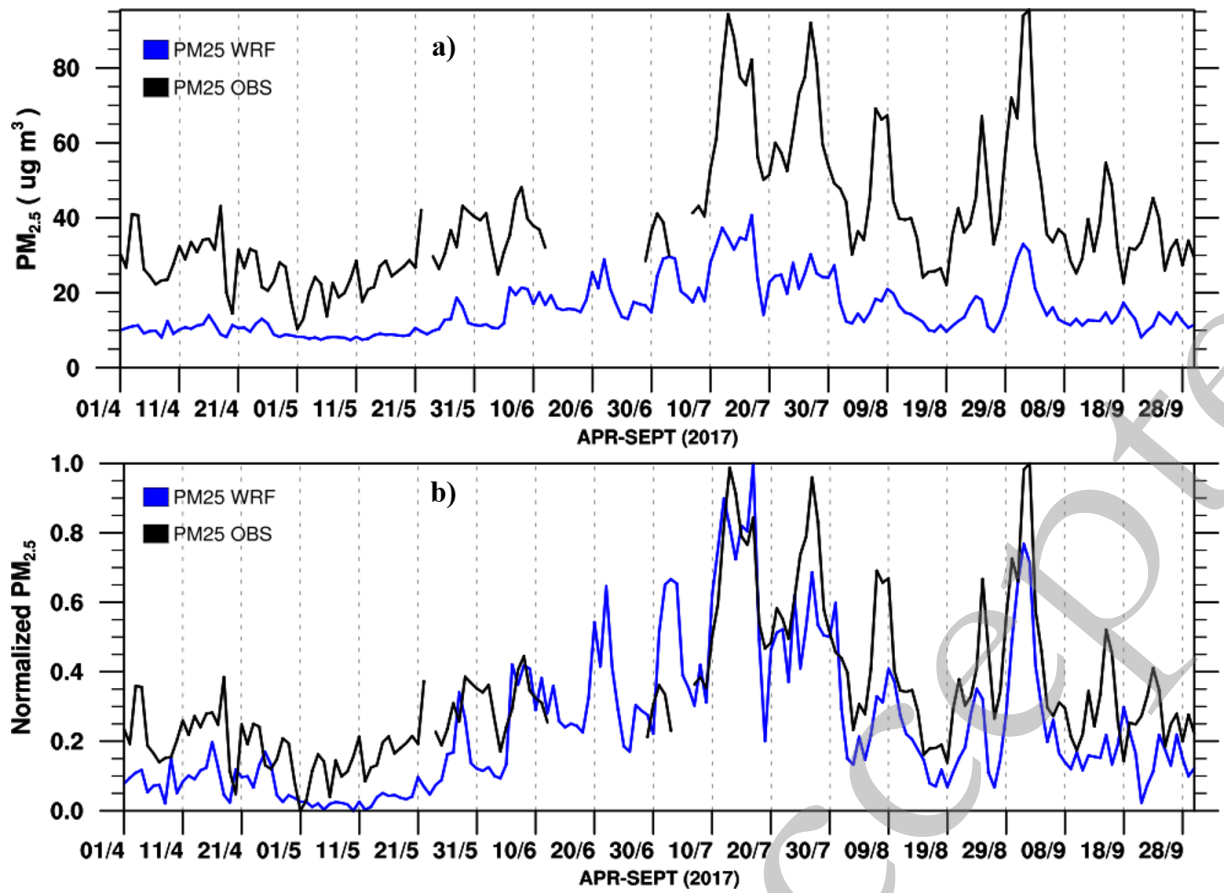

Fig. 6. (a) Daily variations in surface $PM_{2.5}$ concentrations averaged over the stations from WRF-Chem simulations and observations for the April-September period, (b) similar to (a), but the concentrations are normalized by the maximum value during the period for the simulations and observations.

ing consistent peaks and lows (Fig. 6b). The temporal correlation coefficient (r) between the simulations and the observations reaches 0.59. This implies that the simulation can generally capture the fundamental mechanisms driving the temporal variations in surface $PM_{2.5}$ concentrations but may have systematic negative biases, such as underestimating local anthropogenic emissions. This dramatic seasonal variation in surface $PM_{2.5}$ concentration was also reported in previous studies of observations [73, 74]. In the next section, further analyses are conducted to evaluate the causes of these dramatic variations in concentrations during the seasonal transition period (i.e., May, June and July).

3.3 Factors influencing the variation in surface $PM_{2.5}$ concentration

3.3.1 Contribution analysis

To further understand the mechanisms driving the simulated seasonal variation in $PM_{2.5}$ concentrations from April to September in the region with a focus on the transitional period of May (the end of the rainy season), June (beginning of the dry season), and July (with the peak of $PM_{2.5}$ concentrations). The monthly variations in contributions to the $PM_{2.5}$ concentrations from individual processes, such as transport, emission, wet and dry deposition, PBL mixing, and chemical production/loss, were analyzed, and the processing analysis followed the method of [36].

Figure 7 shows the monthly averaged contribution from individual processes to the variation in surface $PM_{2.5}$ concentrations (Fig. 7a), the monthly tendency of surface $PM_{2.5}$ concentrations and the sum contribution from all processes averaged over the city of Kigali (Fig. 7b). The analysis of process contributions is verified by comparing the variations in surface $PM_{2.5}$ concentrations with the sum of the contributions from each process. The tendency represents the sum of all processes and is consistent with the variations in surface $PM_{2.5}$ concentrations. The contributions from transport, emissions, PBL mixing and chemistry are positive, while the contributions from wet deposition and dry position are negative during May, June, and July. The monthly tendency mainly indicates an increase in $PM_{2.5}$ concentrations from June to July. The monthly variation in $PM_{2.5}$ concentrations is mainly governed by the variation in contributions from transport, dry deposition and PBL mixing. The contribution from emissions remains constant during May, June, and July. The chemical production is highest in July, which is associated with the highest photochemical activity. The contribution from transport is negative in May, which can be related to less or no aerosols being transported across the region to the city, while it is positive from June to July, which is mainly attributed to the regional transport of biomass burning aerosols nearby. The contribution from dry deposition increases from May to July due to increased solar radiation during June and July and near-surface wind. The wet deposition contribution is high in May

DOI: 10.52396/JUSTC-2022-0142
JUSTC, **2023**, 53(5):

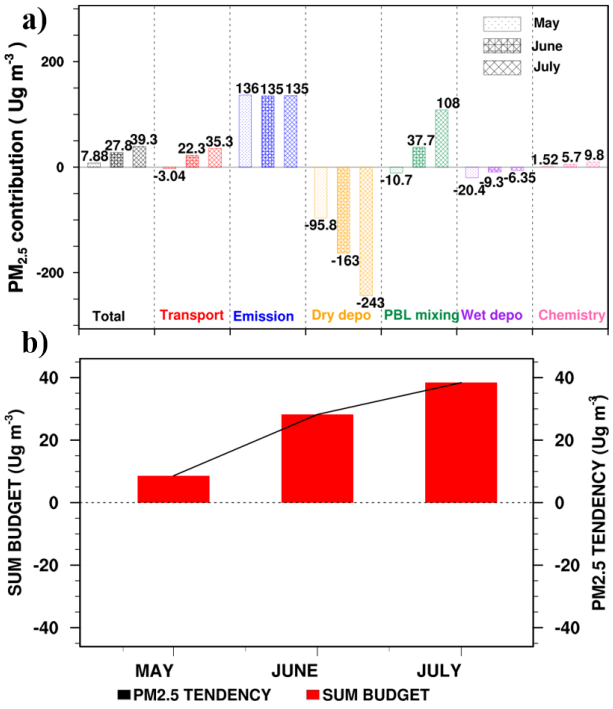

Fig. 7. (a) Contribution of the individual processes (transport, emission, wet and dry deposition, chemical production/loss, PBL mixing) to $PM_{2.5}$ concentrations averaged over Kigali. (b) Total budget analysis averaged over Kigali. Red bars represent the sum of individual processes, and the black line represents the tendency of $PM_{2.5}$ concentrations during May, June and July.

and lowest in July due to less or no rainfall during the dry season (month of July) (Fig. 11b). The PBL mixing is negative in May and peaks in July, entrained strong downward mixing of transported aerosols from the southwestern region over the city of Kigali and increased the $PM_{2.5}$ concentrations. The combined effect of emissions, transport, dry deposition, and PBL mixing represents the overall tendency (black column, Fig. 7a). It can be noted that dry deposition, wet deposition, transport, and PBL mixing are the determinant processes leading to $PM_{2.5}$ concentration variation.

To further demonstrate the contribution of each component to the seasonal variation in surface $PM_{2.5}$ concentrations, Figure 8 shows the monthly variation in each component averaged for May, June and July. The results reveal that EC, OC and OIN increased significantly from May to July and contributed to a large portion of the total concentration throughout the period. There was a sharp increase in OC and OIN concentrations from June to July, and they contributed to more than 80% of the total $PM_{2.5}$ concentration. The OC concentration increases from May (wet season) to June-July (dry season), and OIN increases from June and peaks in July. The trend of surface $PM_{2.5}$ concentrations agrees with the tendency of contributions from budget analysis, accounting for 8.84 $\mu g \cdot m^{-3}$, 28.3 $\mu g \cdot m^{-3}$, and 38.5 $\mu g \cdot m^{-3}$ in May, June and July, respectively. Therefore, the variability in the surface $PM_{2.5}$ concentration is mainly associated with the variation in EC, OC, and OIN throughout the period.

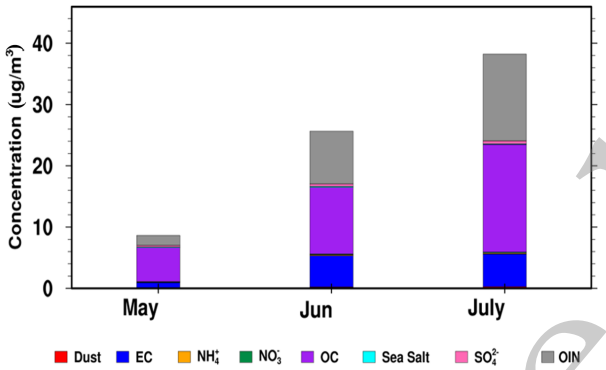

Fig. 8. Monthly average variation in surface $PM_{2.5}$ concentration components (dust, EC, OIN, sea salt, OC, sulfate, ammonium, nitrates) averaged over Kigali during May, June and July.

3.3.2 *Impact of transport*

Generally, the wind circulation over East Africa is mainly governed by the migration of the ITCZ (Dominique Nganga and Gaston Samba, 2011) and the effect of orography and rift valley systems [75, 76]. The monthly mean wind fields at 700 hPa from the ERA-5 reanalysis and the simulations for May, June, and July are shown in Figure 9 to depict the transport of aerosols to downwind regions, as the transport among processes contributed to the variation in PM2.5 concentrations from the budget analysis in Figure 7. Both the reanalysis and simulations show similar wind circulation patterns. Generally, the southeasterly winds dominate the region throughout the period. The period of May is characterized by strong southeasterly winds from the Indian Ocean, while June and July are characterized mostly by southerly winds. The change in wind direction over the southern regions favored the transport of aerosols to Rwanda during July over May. During June and July, southerly winds blow from southern Africa carrying biomass burning aerosols (Fig. 2c), in addition to increased anthropogenic activities during the local dry season, which release a significant amount of smoke particles transported downwind to Rwanda [68], leading to high concentrations of EC, OC and OIN during the June-July period (Fig. 8).

3.3.3 *Impact of PBL mixing*

The variation in surface $PM_{2.5}$ concentration is strongly affected by meteorological factors, as discussed above in the budget analysis, among which PBL mixing plays an important role during May, June, and July. Figure 10 presents the monthly variation in PBLH from boxplot analysis averaged over the city of Kigali. The PBLH shows a typical seasonal trend with low values in May and high values in July, reaching its lowest values at approximately 300 m in May and June and its highest values in July at approximately 700 m. This seasonal variation in the PBLH, with a maximum in summer and a minimum in winter, can be attributed to higher solar radiation and heat flux in July and leads to stronger surface heating and stronger turbulence and convection within the boundary layer during the period of July. Stronger PBL mixing normally leads to larger upward and downward turbulent transport of particles between upper levels and the ground level. The net effect is determined by whether the concentration at the ground level is higher than that at the upper level. In general, without long-range transport, the contribution

DOI: 10.52396/JUSTC-2022-0142
JUSTC, **2023**, 53(5):

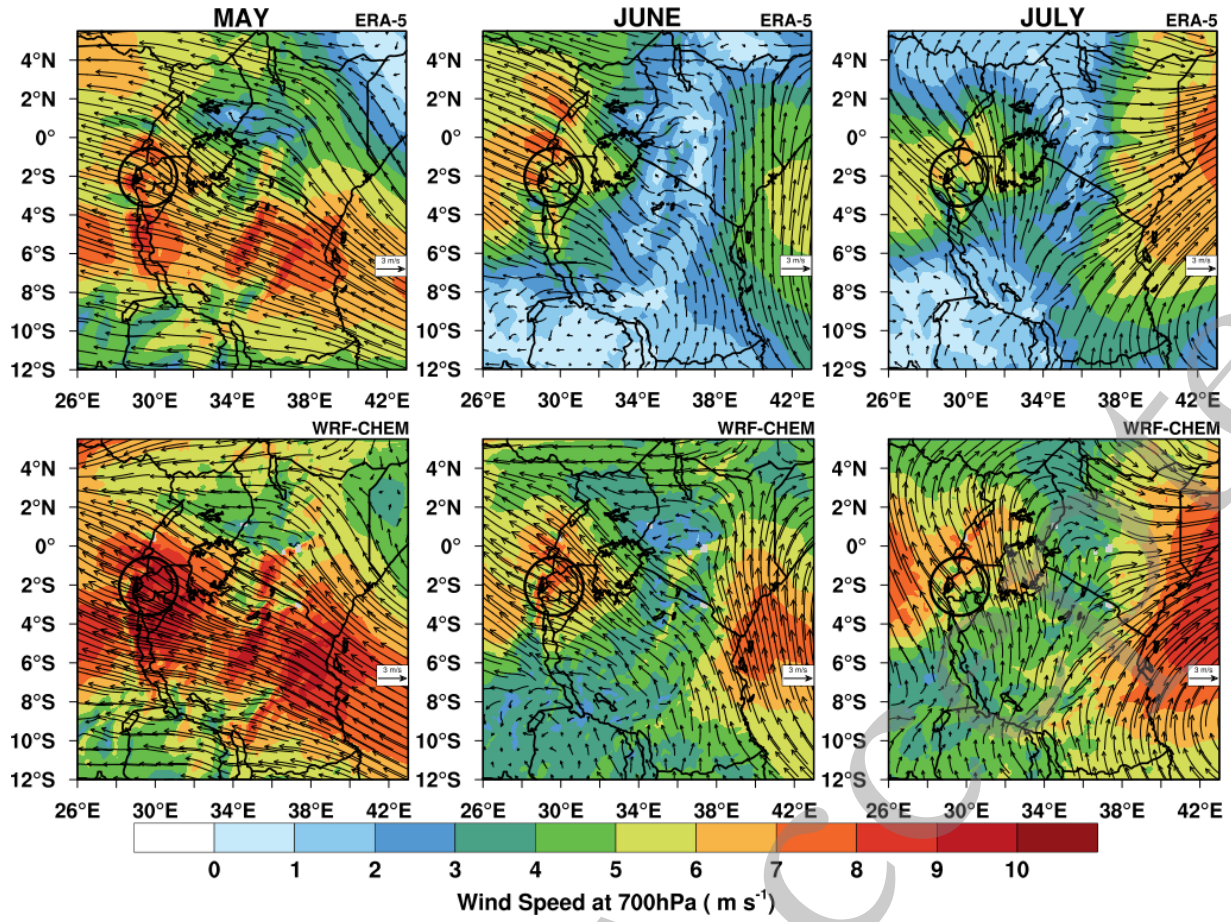

Fig. 9. Monthly average wind circulation pattern at the 700 hPa level for May, June, and July. The shading contours represent wind speed, and the wind barbs represent wind at 5 $m \cdot s^{-1}$ from WRF-Chem and ERA-5 reanalysis. The black circle represents Rwanda.

from PBL mixing to the surface concentration is negative because mixing will transport the mass from the near-surface to the upper level. The PBL mixing contribution to the surface concentration is positive in June and July, which corresponds well to the positive contribution from transport in June and July (Fig. 7). Furthermore, the linear relationship between PBLH and $PM_{2.5}$ concentrations reveals a positive correlation coefficient in May and June with values of 0.64 and 0.25, respectively, and an anti-correlation during July with a value of −0.34 (see the supporting information, Fig. S2). This result reflects that the concentration in the upper level is higher (lower) than that in the ground level in July (May and June).

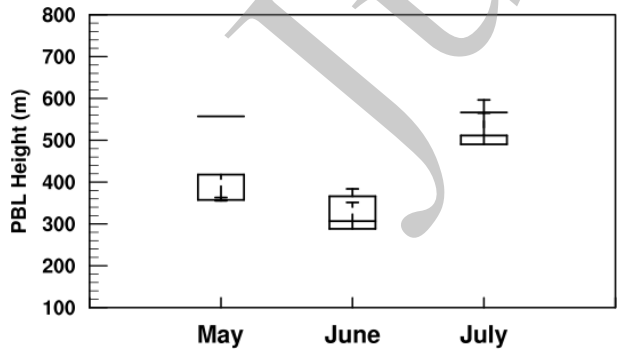

Fig. 10. Monthly variation in PBLH averaged over the city of Kigali during May, June and July.

3.3.4 *Impact of dry and wet deposition*

To understand the impact of dry and wet deposition on the surface $PM_{2.5}$ concentrations, the meteorological factors affecting the dry and wet deposition processes are investigated. Dry deposition can be largely influenced by friction velocity and surface roughness [77]. Figure 11 shows the monthly average wind vectors at 10 m collocated with friction velocity and monthly average rainfall during May, June and July from the WRF-Chem simulations. The southeasterly winds dominated the circulation over the region, and the mean wind speed over Kigali varied slightly by 2.10 $m \cdot s^{-1}$, 1.9 $m \cdot s^{-1}$ and 2.15 $m \cdot s^{-1}$ in May, June and July, respectively. The friction velocity also increases from 0.24 to 0.27 $m \cdot s^{-1}$ from May to July. The dry deposition velocity strongly depends on the wind speed; thus, the higher the wind speed is, the higher the friction velocity, which accelerates the transport of particulate matter over the city of Kigali, thus contributing to the reduction in the $PM_{2.5}$ concentration throughout the period (Fig. 7a). Note that the monthly mean friction velocity and near-surface wind speed increase slightly during June and July; thus, the deposition flux is dominated by wet deposition (Fig. 11b). The rainfall decreases significantly by 0.259 mm hr^{-1}, 0.108 mm hr^{-1} and 0.041 $mm \cdot hr^{-1}$ for May, June and Juy, respectively (see also the supporting information, Fig. S3), which explains an increase in $PM_{2.5}$ concentrations with higher washout of aerosols in May and less or no washout in July (Fig. 7a).

DOI: 10.52396/JUSTC-2022-0142
JUSTC, **2023**, 53(5):

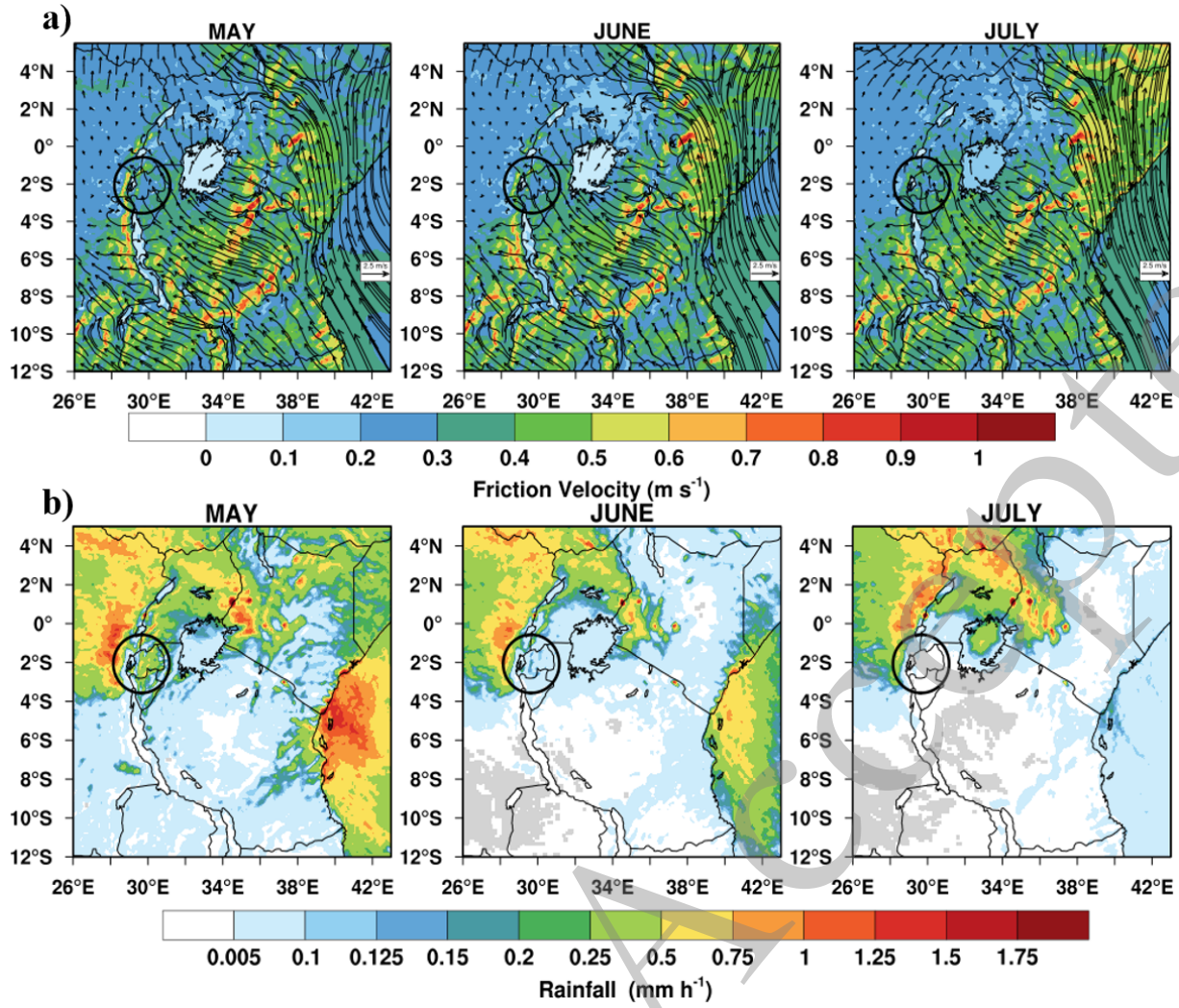

Fig. 11. (a) Monthly average friction velocity and 10 m wind field pattern for May, June, and July. shading contours represent friction velocity and wind barbs represent wind speed at 2.5 m·s^{-1} from WRF-Chem (b) Monthly average of spatial distribution of rainfall for May, June and July period from WRF-Chem simulations, the black circle represents Rwanda.

4 Conclusions

In this study, the seasonal variation in surface $PM_{2.5}$ concentrations over East Africa over six months based on the observed and simulated daily $PM_{2.5}$ concentrations in Kigali city in the western region of East Africa is analyzed. The mechanisms driving the variation are investigated. On average, the observed concentration is low in the rainy season (May) and peaks in the dry season (July). WRF-chem simulations generally capture the seasonal variation in $PM_{2.5}$ concentrations from April to September but underestimate the concentrations throughout the period, likely due to the uncertainties in local and regional emissions over East Africa. The lowest surface $PM_{2.5}$ concentration is found during the wet season (May) with 10 μg m^{-3} and 20 μg m^{-3} from the simulation and the observation, respectively, while the highest concentration is found during the dry season (July, August) with 45 μg m^{-3} and 90 μg m^{-3} from the simulation and the observation, respectively. The simulation can generally reproduce the pollution episodes during the dry season. Consistent with the surface PM2.5 concentration, a higher AOD is observed during the dry season (JJAS), and a lower AOD is observed during the wet season (AM).

The analysis of the process contributions to the surface $PM_{2.5}$ concentrations reveals that PBL mixing, dry and wet deposition, and transport are the dominant processes controlling the seasonal variation in surface $PM_{2.5}$ concentrations over East Africa. The composition analysis of surface $PM_{2.5}$ concentrations reveals that OIN and OC are the dominant components accounting for 80% and 15% of surface PM2.5 concentrations, respectively, and drive the seasonal variation. The contribution of the transport process to the surface PM2.5 concentration changes from negative in May to positive in June and July, mainly due to the change in wind direction from southeasterly winds in May to southerly winds in July over the western region of East Africa (e.g., Rwanda), which results in a positive contribution from the transported biomass burning aerosols to East Africa. The contribution of the PBL mixing process is controlled by both the strength of turbulence (generally increasing from May to July) and the transported aerosols in the upper level over East Africa. The higher PBLH and stronger turbulent mixing in July entrained

DOI: 10.52396/JUSTC-2022-0142
JUSTC, **2023**, 53(5):

more transported aerosols from southern Africa downward toward the surface, which resulted in a change in the negative contribution of PBL mixing in May to a positive contribution in July. Moreover, the contribution of the dry deposition process increases with increasing surface concentration from May to July, although the dry deposition rate changes slightly. The contribution of wet deposition decreases significantly from May to July due to the decrease in rainfall amounts.

This study highlighted the usage of the WRF-Chem model in investigating the temporal and spatial variations in surface $PM_{2.5}$ concentrations over East Africa, representing the first work of modeling and investigating the $PM_{2.5}$ concentrations over this area. However, please note that this study only focuses on the observations of one city because the observational data over the region are very scarce. Future work would require observations of $PM_{2.5}$ concentrations and their compositions at different sites over the East Africa region for further characterization of seasonal variations in $PM_{2.5}$ concentrations over a broad area. More observations are also needed to constrain regional/local emissions over the region, which is also important to improve our understanding of the impacts of multiple processes, such as chemical production, emissions and meteorological factors, on the evolution of air pollution in the region.

Supplemental information

The supplemental information includes 3 figures.

Data availability

The release version of WRF-chem can be downloaded from http://www2.mmm.ucar.edu/wrf/users/download/get_source.html. The updated USTC version of WRF-chem can also be downloaded from http://aemol.ustc.edu.cn/product/list/ or can contact chunzhao@ustc.edu.cn. Code modifications will be incorporated in the release version of WRF-chem in the future.

Acknowledgements

This research was supported by the Strategic Priority Research Program of the Chinese Academy of Sciences (XDB41000000), the Fundamental Research Funds for the Central Universities, the USTC Research Funds of the Double First-Class Initiative, and the National Natural Science Foundation of China (42061134009, 41775146). The study used computing resources from the High-Performance Computing Center of the University of Science and Technology of China (USTC) and TH-2 of the National Supercomputer Center in Guangzhou (NSCC-GZ). Special appreciation goes to the University of Rwanda and Carnegie-Mellon University for procuring observation data. The authors are also indebted to the principal investigator Prof. Brent Holben (NASA) and staff for establishing and maintaining the AERONET site data used in this study. We are grateful to the MODIS and MISR support teams for processing satellite data.

Conflict of Interest

The authors declare that there are no conflicts of interest to report.

Funding Information

This research was supported by the Strategic Priority Research Program of the Chinese Academy of Sciences (grant XDB41000000), the Fundamental Research Funds for the Central Universities, the USTC Research Funds of the Double First-Class Initiative, and the National Natural Science Foundation of China (42061134009, 41775146).

References

[1] IPCC (2022) Climate Change 2022 Mitigation of Climate Change. Working Group III contribution to the Sixth Assessment Report of the Intergovernmental Panel on Climate Change, IPCC AR6 WG III, 2022.

[2] Ma J, Xu X, Zhao C, Yan P. A review of atmospheric chemistry research in China: Photochemical smog. *haze pollution, and gas-aerosol interactions. Adv. Atmos. Sci.,* **2012**, *29* (5): 1006–1026.

[3] Lin, Neng, Huei, Chang, Moo, Been, Hwang J, Kaneyasu N, Zhang R (2018) Overview of the Special Issue "Aerosol Source, Transport, Chemistry, and Emission Control" for the 10th Asian Aerosol Conference 2017. Aerosol Air Qual. Res. 18(7): 1515–1518.

[4] IPCC (2013) Climate Change 2013 The Physical Science Basis. Working Group I contribution to the fifth assessment report of the Intergovernmental Panel on Climate Change, IPCC AR5 WG I. Intergovernmental Panel on Climate Change, New York.

[5] IPCC (2007) The physical science basis : summary for policymakers: contribution of Working Group I to the Fourth assessment report. of the Intergovernmental Panel on Climate Change. IPCC, Geneva.

[6] WHO (ed) (2013) Ambient air pollution: A global assessment of exposure and burden of diseases.

[7] Pope, Francis, D., Gatari M, Ng'anga D, Poynter A, Blake R. Airborne particulate matter monitoring in Kenya using calibrated low-cost sensors. *Atmos. Chem. Phys.,* **2018**, *18* (20): 15403–15418.

[8] UK DFID (2018) East African Regional Analysis of Youth Demographics.

[9] Doumbia M, Toure N'D, Silue S, Yoboue V, Diedhiou A, Hauhouot C. Emissions from the Road Traffic of West African Cities: Assessment of Vehicle Fleet and Fuel Consumption. *Energies,* **2018**, *11* (9): 2300.

[10] Kalisa E, Nagato EG, Bizuru E, Lee KC, Tang N, Pointing SB, Hayakawa K, Archer SDJ, Lacap-Bugler DC (2018) Characterization and Risk Assessment of Atmospheric PM2.5 and PM10 Particulate-Bound PAHs and NPAHs in Rwanda, Central-East Africa. Environmental science & technology 52(21): 12179–12187.

[11] Kirenga BJ, Meng Q, van Gemert F, Aanyu-Tukamuhebwa H, Chavannes N, Katamba A, Obai G, van der Molen T, Schwander S, Mohsenin V. The State of Ambient Air Quality in Two Ugandan Cities: A Pilot Cross-Sectional Spatial Assessment. *International journal of environmental research and public health,* **2015**, *12* (7): 8075–8091.

[12] Yang W, Seager R, Cane MA, Lyon B. The East African Long Rains in Observations and Models. *J. Climate,* **2014**, *27* (19): 7185–7202.

[13] Camberlin P, Okoola RE. The onset and cessation of the "long rains" in eastern Africa and their interannual variability. *Theor. Appl. Climatol.,* **2003**, *75* (1): 43–54.

[14] García MÁ, Sánchez ML, Los Ríos A de, Pérez IA, Pardo N, Fernández-Duque B (2019) Analysis of PM10 and PM2.5

DOI: 10.52396/JUSTC-2022-0142
JUSTC, **2023**, 53(5):

Concentrations in an Urban Atmosphere in Northern Spain. Archives of environmental contamination and toxicology 76(2): 331–345.

[15] Komkoua-Mbienda AJ, Tchawoua C, Vondou DA, Choumbou P, Kenfack Sadem C, Dey S. Impact of anthropogenic aerosols on climate variability over Central Africa by using a regional climate model. *Int. J. Climatol.*, **2017**, *37* (1): 249–267.

[16] Dezfuli AK, Nicholson SE. The Relationship of Rainfall Variability in Western Equatorial Africa to the Tropical Oceans and Atmospheric Circulation. *Part II:The Boreal Autumn. J. Climate,* **2013**, *26* (1): 66–84.

[17] Hu Y, Li D, Liu J (2007) Abrupt seasonal variation of the ITCZ and the Hadley circulation. Geophys. Res. Lett. 34(18).

[18] Ilunga L, Muhire I, Mbaragijimana C (2004) Pluviometric seasons and rainfall origin in Rwanda. Geo-Eco-Trop: 61–68.

[19] Mutemi JN (2003) Climate anomalies over eastern Africa associated with various ENSO evolution phases. PhD. Thesis, , University of Nairobi, Kenya.

[20] Gaita SM, Boman J, Gatari MJ, Wagner A, Jonsson SK. Characterization of Size-Fractionated Particulate Matter and Deposition Fractions in Human Respiratory System in a Typical African City: Nairobi. *Kenya. Aerosol Air Qual. Res.*, **2016**, *16* (10): 2378–2385.

[21] Mkoma SL, Chi X, Maenhaut W (2010) Characteristics of carbonaceous aerosols in ambient PM10 and PM2.5 particles in Dar es Salaam, Tanzania. The Science of the total environment 408(6): 1308–1314.

[22] Solmon F, Elguindi N, Mallet M (2012) Radiative and climate effects of dust over West Africa, as simulated by a regional climate model: 97–113.

[23] Zhao C, Liu X, Ruby Leung L, Hagos S. Radiative impact of mineral dust on monsoon precipitation variability over West Africa. *Atmos. Chem. Phys.*, **2011**, *11* (5): 1879–1893.

[24] Zhao C, Liu X, Leung LR, Johnson B, McFarlane SA, Gustafson WI, Fast JD, Easter R. The spatial distribution of mineral dust and its shortwave radiative forcing over North Africa: modeling sensitivities to dust emissions and aerosol size treatments. *Atmos. Chem. Phys.*, **2010**, *10* (18): 8821–8838.

[25] Molepo KM, Abiodun BJ, Magoba RN. The transport of PM10 over Cape Town during high pollution episodes. *Atmospheric Environment,* **2019**, *213*: 116–132.

[26] Kuik F, Lauer A, Beukes JP, van Zyl PG, Josipovic M, Vakkari V, Laakso L, Feig GT. The anthropogenic contribution to atmospheric black carbon concentrations in southern Africa: a WRF-Chem modeling study. *Atmos. Chem. Phys.*, **2015**, *15* (15): 8809–8830.

[27] Otieno G, Mutemi JN, Opijah FJ, Ogallo LA, Omondi MH. The Sensitivity of Rainfall Characteristics to Cumulus Parameterization Schemes from a WRF Model. *Part I:A Case Study Over East Africa During Wet Years. Pure Appl. Geophys.*, **2020**, *177* (2): 1095–1110.

[28] Kerandi N, Arnault J, Laux P, Wagner S, Kitheka J, Kunstmann H. Joint atmospheric-terrestrial water balances for East Africa: a WRF-Hydro case study for the upper Tana River basin. *Theor Appl Climatol,* **2018**, *131* (3-4): 1337–1355.

[29] Komkoua Mbienda AJ, Tchawoua C, Vondou DA, Choumbou P, Kenfack Sadem C, Dey S. Sensitivity experiments of RegCM4 simulations to different convective schemes over Central Africa. *Int. J. Climatol.*, **2017**, *37* (1): 328–342.

[30] Cook KH, Vizy EK. The Congo Basin Walker circulation: dynamics and connections to precipitation. *Clim Dyn,* **2016**, *47* (3-4): 697–717.

[31] Pohl B, Crétat J, Camberlin P. Testing WRF capability in simulating the atmospheric water cycle over Equatorial East Africa. *Clim Dyn,* **2011**, *37* (7-8): 1357–1379.

[32] Beck V, Koch T, Kretschmer R, Marshall J, Ahmadov R, Gerbig C, Pillai D (2011) The WRF Greenhouse Gas Model (WRF-GHG) Technical Report No. 25. Max Planck Institute for Biogeochemistry, Jena.

[33] Skamarock W, Klemp, J. , B. , Dudhia J, Gill, D. , O. , Barker DM, Duda, M. , G. , Huang, X. , Y. , Wang W, and Powers, J. , G. (2008) A Description of the Advanced Research WRF Version 3. American Journal of Climate Change.

[34] Grell GA, Peckham SE, Schmitz R, McKeen SA, Frost G, Skamarock WC, Eder B. Fully coupled online chemistry within the WRF model. *Atmospheric Environment,* **2005**, *39* (37): 6957–6975.

[35] Zhang M, zhao c, Yang Y, Du Q, Shen Y, Lin S, Gu D (2021) Sensitivity of different BVOC emission schemes in WRF-Chem(v3.6) to vegetation distributions and its impacts over East China. Geosci. Model Dev.

[36] Du Q, zhao c, Zhang M, Dong X, Chen Y, Liu Z, Hu Z, Zhang Q, Li Y, Yuan R, Miao S (2020) Modeling diurnal variation of surface $PM_{2.5}$ concentrations over East China with WRF-Chem: impacts from boundary-layer mixing and anthropogenic emission. Atmos. Chem. Phys. 20(5): 2839–2863.

[37] Hu Z, Huang J, zhao c, Bi J, Jin Q, Qian Y, Leung LR, Feng T, Chen S, Ma J. Modeling the contributions of Northern Hemisphere dust sources to dust outflow from East Asia. *Atmospheric Environment,* **2019**, *202*: 234–243.

[38] Zhao C, Huang M, Fast, Jerome, D., Berg, Larry, K., Qian Y, Guenther A, Gu D, Shrivastava M, Liu Y, Walters S, Pfister G, Jin J, Shilling JE, Warneke C. Sensitivity of biogenic volatile organic compounds to land surface parameterizations and vegetation distributions in California. *Geosci. Model Dev.*, **2016**, *9* (5): 1959–1976.

[39] Zhao C, Hu Z, Qian Y, Leung LR, Huang J, Huang M, Jin J, Flanner M, Zhang R, Wang H, Yan H, Lu Z, and Streets, D. G. Simulating black carbon and dust and their radiative forcing in seasonal snow: a case study over North China with fieldcampaign measurements. . *Atmos. Chem. Phys.*, **2014**, *14* (2): 11475–11491.

[40] Fast JD, Gustafson Jr. , W. I. , Easter RC, Zaveri RA, Barnard JC, Chapman EG (2006) Evolution of ozone, particulates, and aerosol direct forcing in an urban area using a new fully coupled meteorology, chemistry, and aerosol model, . J. Geophys. Res 111.

[41] Francis S. Binkowski, Uma Shankar The Regional Particulate Matter Model 1. Model description and preliminary results.

[42] Easter R, Liu X, Ghan S, Zaveri R, Gettelman A, Rasch P (2009) Influence of anthropogenic sulfate and black carbon on upper tropospheric clouds in the NCAR CAM3 model coupled to the IMPACT global aerosol model, . J. Geophys. Res. 114(D03204).

[43] Zhao C, Ruby Leung, Easter R, Hand J, Avise J. Characterization of speciated aerosol direct radiative forcing over California. *J. Geophys. Res. Atmos.*, **2013**, *118* (5): 2372–2388.

[44] Morrison H, Thompson G, Tatarskii V. Impact of Cloud Microphysics on the Development of Trailing Stratiform Precipitation in a Simulated Squall Line: Comparison of One- and Two-Moment Schemes. *Mon. Wea. Rev.*, **2009**, *137* (3): 991–1007.

[45] Hong Y, Dudhia J. A new vertical diffusion package with an explicit treatment of entrainment processes. *Mon. Wea. Rev.*, **2006**, *134*: 2318–2341.

[46] Kain JS. The Kain–Fritsch Convective Parameterization: An Update. *J. Appl. Meteor.*, **2004**, *43* (1): 170–181.

[47] Mlawer EJ, Taubman SJ, Brown PD, Iacono MJ, Clough SA. Radiative transfer for inhomogeneous atmospheres: RRTM. *a validated correlated-k model for the longwave. J. Geophys. Res.,* **1997**, *102* (D14): 16663–16682.

[48] Iacono MJ, Mlawer EJ, Clough SA, Morcrette J-J (2000) Impact of an improved longwave radiation model, RRTM, on the energy budget and thermodynamic properties of the NCAR community climate model, CCM3. J. Geophys. Res. 105(D11): 14873–14890.

[49] Zhao C, Chen S, Kok J, Leung LR, Qian Y, Huang J, Zaveri R. Uncertainty in modeling dust mass balance and radiative forcing from size parameterization. . *Atmos. Chem. Phys.*, **2013**, *13*: 10733–10753.

[50] Seaman NL, Stauffer DR, Lario-Gibbs AM. A Multiscale Four-Dimensional Data Assimilation System Applied in the San Joaquin

DOI: 10.52396/JUSTC-2022-0142
JUSTC, **2023**, 53(5):

Valley during SARMAP. *Part I:Modeling Design and Basic Performance Characteristics, . J. Appl. Meteor.,* **1995**, *34*: 1739–1761.

[51] Liu P, Tsimpidi AP, Hu Y, Stone B, Russell AG, Nenes A. Differences between downscaling with spectral and grid nudging using WRF. *Atmos. Chem. Phys.,* **2012**, *12* (8): 3601–3610.

[52] Stauffer DR, Seaman, Nelson, L. Use of Four-Dimensional Data Assimilation in a Limited-Area Mesoscale Model. *Part I:Experiments with Synoptic-Scale Data. Mon. Wea. Rev.,* **1990**, *118* (6): 1250–1277.

[53] Janssens-Maenhout G, Crippa M, Guizzardi D, Dentener F, Muntean M, Pouliot G, Keating T, Zhang Q, Kurokawa J, Wankmüller R, Van der Denier Gon, H. , Kuenen J (2015) HTAP_v2.2: a mosaic ofregional and global emission grid maps for 2008 and 2010 to study hemispheric transport of air pollution. Atmos. Chem. Phys. 15: 11411–11432.

[54] Wiedinmyer C, Akagi SK, Yokelson RJ, Emmons LK, Al-Saadi JA, Orlando JJ, and Soja AJ. The Fire INventory from NCAR (FINN) – a high resolution global model to estimate the emissions from open burning. . *Geosci. Model Dev.,* **2010**, *3*: 2439–2476.

[55] Dentener F, Kinne S, Bond T, Boucher O, Cofala J, Generoso S, Ginoux P, Gong S, Hoelzemann JJ, Ito A, Marelli L, Penner JE, Putaud J-P, Textor C, Schulz M, van der Werf GR, Wilson J. Emissions of primary aerosol and precursor gases in the years 2000 and 1750. *prescribed data-sets for AeroCom. Atmos. Chem. Phys. Discuss.,* **2006**, *6* (2): 2703–2763.

[56] Gong SL. A parameterization of sea-salt aerosol source function for sub- and supermicron particles. *Global Biogeochem. Cycles,* **2003**, *17* (4): n/a–n/a.

[57] Jaeglé L, Quinn, P., K., Bates, T., S., Alexander B, Lin, J., T. Global distribution of sea salt aerosols: new constraints from in situ and remote sensing observations. . *Atmos. Chem. Phys.,* **2011**, *11*: 3137–3157.

[58] Ginoux P, Chin M, Tegen I, Prospero JM, Holben B, Dubovik O, Lin S-J. Sources and distributions of dust aerosols simulated with the GOCART model. *J. Geophys. Res.,* **2001**, *106* (D17): 20255–20273.

[59] Kok JF. A scaling theory for the size distribution of emitted dust aerosols suggests climate models underestimate the size of the global dust cycle. *Proceedings of the National Academy of Sciences of the United States of America,* **2011**, *108*: 1016–1021.

[60] Kaufman YJ, Tanré D, Boucher O. A satellite view of aerosols in the climate system. *Nature,* **2002**, *419* (6903): 215–223.

[61] Kaufman YJ, Tanré D, Remer LA, Vermote EF, Chu A, Holben BN. Operational remote sensing of tropospheric aerosol over land from EOS moderate resolution imaging spectroradiometer. *J. Geophys. Res.,* **1997**, *102* (D14): 17051–17067.

[62] Sayer AM, Munchak LA, Hsu NC, Levy RC, Bettenhausen C, Jeong M-J. MODIS Collection 6 aerosol products: Comparison between Aqua's e-Deep Blue. *Dark Target, and "merged" data sets, and usage recommendations. J. Geophys. Res. Atmos.,* **2014**, *119* (24): 13,965–13,989.

[63] Martonchik JV (2004) Comparison of MISR and AERONET aerosol optical depths over desert sites. Geophys. Res. Lett. 31(16).

[64] Holben BN, Eck TF, Slutsker I, Tanré D, Buis JP, Setzer A, Vermote E, Reagan JA, Kaufman YJ, Nakajima T, Lavenu F, Jankowiak I, Smirnov A. AERONET —A Federated Instrument Network and Data Archive for Aerosol Characterization. *Remote Sensing of Environment,* **1998**, *66* (1): 1–16.

[65] Zimmerman N, Presto AA, Kumar SPN, Gu J, Hauryliuk A, Robinson ES, Robinson AL, Subramanian R (2017) Closing the gap on lower cost air quality monitoring: machine learning calibration models to improve low-cost sensor performance.

[66] Subramanian R (2017) community air quality monitoring with the ramp sensor package. Accessed 12-May-2020.

[67] Ntwali D, Chen H. Diurnal spatial distributions of aerosol optical and cloud micromacrophysics properties in Africa based on MODIS observations. *Atmospheric Environment,* **2018**, *182*: 252–262.

[68] DeWitt HL, Gasore J, Rupakheti M, Potter KE, Prinn RG, Ndikubwimana JdD, Nkusi J, Safari B. Seasonal and diurnal variability in O 3. *black carbon, and CO measured at the Rwanda Climate Observatory. Atmos. Chem. Phys.,* **2019**, *19* (3): 2063–2078.

[69] Boiyo R, Kumar KR, Zhao T, Bao Y. Climatological analysis of aerosol optical properties over East Africa observed from space-borne sensors during 2001–2015. *Atmospheric Environment,* **2017**, *152*: 298–313.

[70] Boiyo R, Kumar KR, Zhao T. Optical. *microphysical and radiative properties of aerosols over a tropical rural site in Kenya, East Africa:Source identification, modification and aerosol type discrimination. Atmospheric Environment,* **2018**, *177*: 234–252.

[71] Kumar KR, Attada R, Dasari HP, Vellore RK, Langodan S, Abualnaja YO, Hoteit I. Aerosol Optical Depth variability over the Arabian Peninsula as inferred from satellite measurements. *Atmospheric Environment,* **2018**, *187*: 346–357.

[72] Ngarukiyimana JP, Fu Y, Yang Y, Ogwang BA, Ongoma V, Ntwali D. Dominant atmospheric circulation patterns associated with abnormal rainfall events over Rwanda. *East Africa. Int. J. Climatol,* **2018**, *38* (1): 187–202.

[73] Kalisa E, Archer S, Nagato E, Bizuru E, Lee K, Tang N, Pointing S, Hayakawa K, Lacap-Bugler D (2019) Chemical and Biological Components of Urban Aerosols in Africa: Current Status and Knowledge Gaps. International journal of environmental research and public health 16(6).

[74] Nahayo L, Nibagwire D, Habiyaremye G, Kalisa E, Udahogora M, Maniragaba A. Awareness on Air Pollution and Risk Preparedness among Residents in Kigali City of Rwanda. *International Journal of Sustainable Development & World Policy,* **2019**, *8* (1): 1–9.

[75] Ayugi BO, Tan G. Recent trends of surface air temperatures over Kenya from 1971 to 2010. *Meteorol Atmos Phys,* **2019**, *131* (5): 1401–1413.

[76] Anyah RO (2006) Simulated Physical Mechanisms Associated with Climate Variability over Lake Victoria Basin in East Africa.

[77] Noll, K., E., Fang, K., Y., P. Development of a dry deposition model for atmospheric coarse particles. *Atmospheric Environment,* **1989**, *23* (3): 589–594.

DOI: 10.52396/JUSTC-2022-0142
JUSTC, **2023**, 53(5):